A wheel-rail electrical contact experiment at the laboratory scale

Luna Haydar, Florent Loete, Frédéric Houzé, Philippe Teste, Tanguy Choupin, Fabien Guiche

A wheel-rail electrical contact experiment at the laboratory scale

Haydar, Luna[1,2], Loete, Florent[2], Houzé, Frédéric[2], Testé, Philippe[2], Choupin, Tanguy[1], Guiche, Fabien[3],

[1]SNCF, Direction Technologies Innovation et Projets Groupe, 1-3 avenue François Mitterrand, 92300 La Plaine Saint Denis, France

[2]GeePs, Group of electrical engineering Paris, CNRS, CentraleSupélec, Université Paris-Saclay, 3 & 11 rue Joliot-Curie, 91192 Gif-sur-Yvette Cedex, France

[3]SNCF Réseau, Direction Générale Industrielle & Ingénierie, Direction Technique Réseau, Département de la Signalisation Ferroviaire, 6 avenue François Mitterrand, 93574 La Plaine Saint Denis Cedex, France

Summary

In order to improve the safety of the railway network, accurately knowing the train's location on a track section is an important task. Generally, this can be ensured by the technical system known as "track circuit". The reliability of the track circuit depends on the quality of the electrical contact between the wheel and the rail. Unfortunately, any degradation of the materials (wheel-rail) can result in a malfunction of the track circuit and thus a failure of the train detection, which can be extremely dangerous in terms of the safety of the rail network and passengers. In this paper, the designing and realization of a test bench that reproduces the electrical wheel-rail contact at a laboratory scale is presented. The scaling was done considering mechanical, electrical, and thermal effects. An original homemade salt spray system was elaborated and used to obtain a controlled oxidation of the rail. Some preliminary results of the electrical resistance behavior of the test bench as a function of several parameters (contact force, roughness and surface oxidation) are examined.

Keywords: deshunting, track circuit, wheel/rail electrical contact, oxidation, test bench.

1 Introduction

The accurate localization of trains on railway tracks is crucial for ensuring the safety of railways. This is achieved through a technical device called the "track circuit", which provides real-time information about the presence of the train within a specific track section. When a train enters this zone, its wheels and axle create a short circuit between the two rails, indicating the occupancy of the zone. The signaling systems can be activated

accordingly. Maintaining a high-quality wheel-rail contact is therefore a major issue for ensuring the reliability of the track circuit system and hence the track safety. If this contact is affected by a third body of natural or artificial origin, present in the interface, the train detection can be jeopardized for a certain period, leading to the phenomenon known as "deshunting" and the train presence is no longer detected. Despite the implementation of various devices to prevent [1] or reduce the occurrence of deshunting, many instances are still being detected every year.

The significant impact that deshunting events can have on the railways management and on the occurrence of potentially dangerous situations, such as level crossing failures and rail accidents, has forced researchers to focus their attention on studying the behavior of the wheel-rail electrical contact interface. The composition of the third body present at the wheel-rail interface may be complex, since it can include both external contaminants (dead leaves, frost, sand, oil...) and oxides formed naturally on surfaces [2]. Regarding oxides, composition was investigated using in situ X-ray diffraction. On the rail head, iron oxide, particularly in the form of FeOOH and Fe_3O_4, is the most dominant species [3]. Furthermore, Nakahara *et al.* provide a surface analysis by examining the concentration of oxide near the contact surface and the composition of both oxide and hydroxide [4]. In [5], the mechanical and electrical aspects of the third body (oxide layer) formed in the wheel-rail contact interface are examined through tribological, morphological and microscopic analyses. The study investigates the electrical conductivity, heterogeneity, continuity, and compactness of the third body under both good and poor shunting conditions. Additionally, Fukuda *et al.* establish that several factors, including normal load, current intensity, oxide layer thickness and traffic frequency, can jointly influence the contact resistance [6]. A better understanding of wheel-rail electrical contact was also obtained through the studies that were carried out on a ¼-scale test rig and on-site using an instrumented regional train [7-8]. These studies highlighted the non-linear $U - I$ characteristics, which are strongly dependent on the presence of oxide at the contact interface. These results showed that scaled-down tests were in fact significantly representative compared to full-scale tests, demonstrating the relevance of performing such experiments. However, conducting tests at full-scale or even ¼-scale can be both cumbersome and costly, making it an obstacle to rapid progress in this area of research.

The aim of this work is to develop a laboratory-scale rolling contact test bench that reduces the complexity and cost associated with conducting these experiments, while faithfully reproducing wheel-rail electrical contact on a reduced scale. By analyzing various aspects of contact under reproducible conditions (controlled speed, load, and oxidation state), we seek to improve our knowledge of the deshunting phenomenon. This paper will be focused on the study of the influence of oxidation since it is one of the major causes of deshunting. The first performed tests to validate the bench consisted in investigating the resistance behavior in relation to different parameters such as load, current, and time. Furthermore, the ease of developing controlled surface degradation protocols makes it easier to assess their impact on contact resistance. Overall, our work offers new perspectives and possibilities for improving railway systems.

2 Bench conception

2.1 General principle

The developed setup, presented in Figure 1, consists in a reduced-scale wheel running on a 1 m full-scale rail. An electrical actuator applies a normal force on the wheel axis inducing a pressure on the contact area equivalent to that produced by a real loaded train. The linear motion axis allows the wheel carriage to move along the rail at a controlled, scaled-down speed.

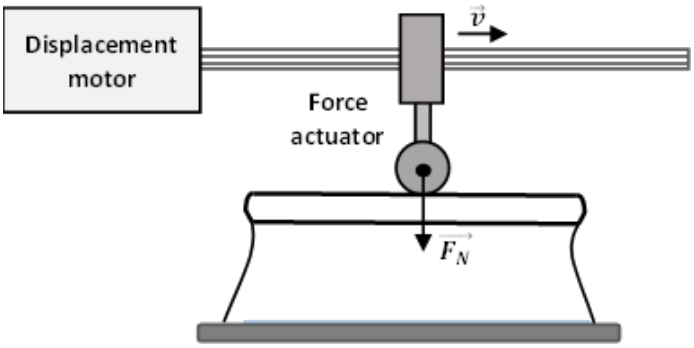

Figure 1: Schematic diagram of the test bench

The bench was designed in order to be the most representative as possible of the devices most likely to be involved in deshunting problems. Electrically, the aim will be to simulate the most extensively used track circuit on the French rail network (FRN).

The sizing of the reduced scale wheel (hereinafter referred to as roller), the load applied, and the speed of the displacement were estimated as explained in section 2.2.

Our major concern was to reproduce the physical behavior of the contact interface. Consequently, we had to study carefully the impact of the downscaling on the dimensions of the setup.

2.2 Dimensioning methodology

Mechanical laws were considered when scaling the test bench to be the most representative of the full-scale behavior of the wheel-rail contact.

It was designed following three criteria:

1. same aspect ratio of the contact surface at both scales.
2. same average contact pressure at both scales.
3. same fraction of contact surface renewed at both scales during a track circuit signal period.

2.2.1. Choice of the roller

The shape of the roller is chosen to ensure that the contact surface between the wheel and the rail is geometrically similar at both scales. To estimate the wheel-rail contact surface, we rely on Hertz's theory, which is a widely-used reference, although we are aware that its assumptions will only be partially satisfied. Hertz's theory assumes:

- Perfectly elastic and homogeneous bodies in contact with isotropic mechanical properties.
- Smooth contact surfaces.
- Semi-infinite bodies with contact dimensions very small compared to body dimensions and radii of curvature.

According to Hertz's theory [9], the contact surface forms an ellipse with semi-axes (*a, b*) and the surface is given by the following expression:

$$S_{contact} = \pi * m * n * \left(\frac{3}{2} * F_N * \left(\frac{1-\upsilon^2}{E}\right) * \left(\frac{1}{A+B}\right)\right)^{\frac{2}{3}} \quad (1)$$

- E and υ: Young's modulus and Poisson's ratio of the steel.
- A and B: combined longitudinal and transverse curvatures.
- m and n: tabulated coefficients dependent on A and B [10].

Consequently, the first criterion means maintaining the same *a/b* ratio between the long and short axes of the elliptical contact surface on both scales.

It is important to note that at full scale, the wheel can be assimilated to a cylinder when it is in contact with the rail (Figure 2, top). Considering that the curvature radius of the head of the rail $R_{c\ rail}$ is unchanged, and the scaling ratio of the wheel, the shape of the contact surface in the transverse direction would have been nearly rectangular. To satisfy the first criterion, the rolling face of the wheel was chosen toroïdal, as pictured in Figure 2, bottom. The transverse radius of curvature $R_{T\ roller}$ allows us to adjust the shape of the contact surface while maintaining the desired *a/b* ratio.

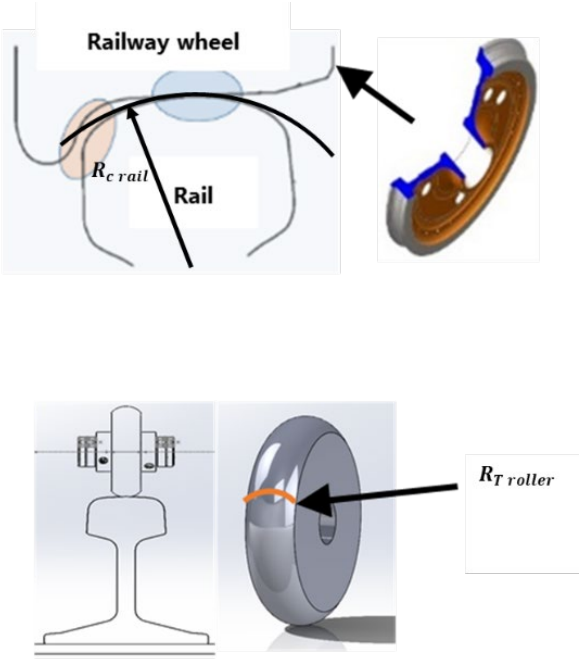

Figure 2: Wheel-rail contact at full scale (top) [13] and at reduced scale (bottom).

2.2.2 Choice of force actuator

According to the second criterion, the choice of the force actuator aims to maintain the same average contact pressure at both scales (denoted respectively $P_{scale\ 1}$ and $P_{reduced\ scale}$) :

$$P_{scale\ 1} = P_{reduced\ scale} \quad (2)$$

Knowing the normal forces per wheel of a full-scale train and its size, and using the Hertz' equation (1), we can calculate the normal force to be applied at the reduced scale using the following equation:

$$F_{N\ reduced\ scale} = P_{scale\ 1} * S_{contact\ reduced\ scale} \quad (3)$$

An abacus has been developed to determine the appropriate normal force required on the reduced scale for a given roller radius, maintaining the same average pressure applied as at full scale. Considering the trains that are the most subject to deshunting, the full scale load per wheel ranges from 55 kN to 105 kN resulting in a 235 N to 430 N range at reduced scale for a 30 mm radius roller.

2.2.3. Speed scaling

Considering the third criterion, the speed of the wheel carriage has to be chosen to maintain the same fraction of contact area renewed during a track circuit signal period at both scales.

The extreme case of this criterion corresponds to the minimum displacement speed at which the contact ellipse will be completely renewed within a track circuit signal period Δt. In this case, the contact interface comprises a "new" oxide layer at each current alternation. The minimum speed required to obtain a fully renewed contact ellipse is denoted by v_{2a}. It can be calculated using the following equation:

$$v_{2a} = 2 * a * f_{cdv} \quad (4)$$

where f_{cdv} is the frequency of the track circuit considered in our study.

2.3 Four-point electrical measurements

The measurement of the wheel-rail electrical contact resistance is performed using the four-point method, as shown in Figure 3-b, which illustrates the principle of this technique applied to the test bench. Figure 3-a shows a photograph of the concrete implementation, where two copper thread brushes are used to inject current from a source into the contact, while two other brushes (placed closest to the contact) are used to measure the contact voltage. The current flowing through the contact is evaluated by measuring the voltage V_s across a well-known shunt resistance R_s.

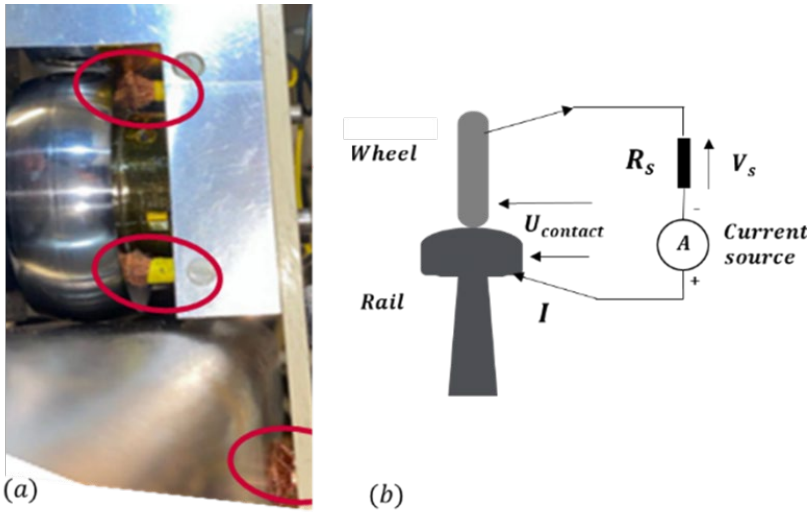

Figure 3: Electrical measurement system based on the four-point method: (a) photograph of the copper thread brushes (circled) (b) schematic of the electrical measurement setup on the bench.

2.4 Surfaces preparation

2.4.1 Reference surfaces

To approach the conditions required by Hertz's theory, where surfaces are assumed to be perfectly smooth, efforts were made to improve the roughness of both the wheel and rail surfaces. In order to obtain a smoother surface, the wheel was polished using different grades of polishing paper. Evaluation of the overall surface quality (surface defects) was performed using a binocular observation, as shown in

. Additionally, a profilometer was then employed to measure the surface roughness. Based on more than 30 measurements, we found that the average and peak-to-peak roughness values were respectively $R_a = 0.4\ \mu m$ and $R_t = 4.5\ \mu m$.

As for the rail, the same polishing process was applied. However, given the complexity of assessing rail surface quality with binocular or profilometer observations, considering its size, a roughness tester from Mitutoyo ('SurfTest SJ301' model) was used. This device can evaluate arithmetic roughness (Ra) and other parameters associated with surface profile parameters. Based on more than 30 measurements within an arbitrary rail zone, the roughness values obtained were $R_a = 0.8\ \mu m$ for average roughness and $R_t = 8.2\ \mu m$ for peak-to-peak roughness.

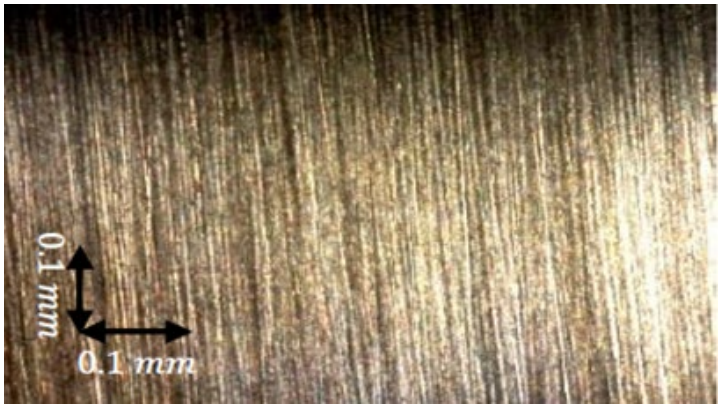

Figure 4: Improved wheel surface quality observed through a binocular lens.

Following this work, six distinct reference zones, shown in Figure 5, were delimited on the wheel where the visual aspect was observed and the roughness measured before and after the experiments, presented in section 3.

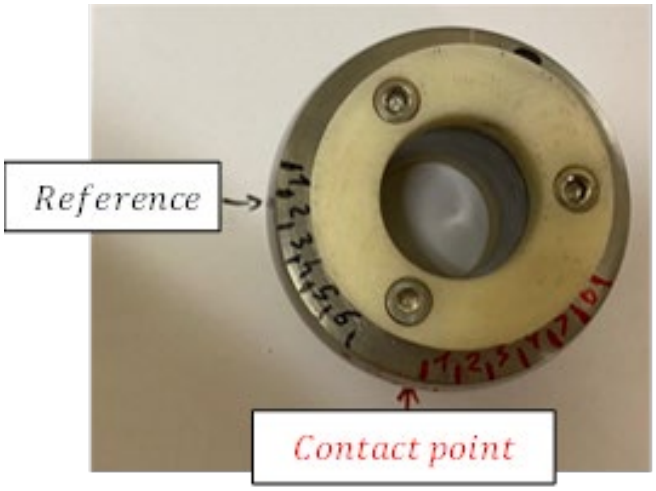

Figure 5: Six reference zones defined on the wheel after an improvement in polishing quality.

2.4.2 Oxidation protocol

To achieve severe, accelerated and controlled oxidation of the rails, we employed a homemade salt spray system. The principle of this system consists of spraying a saline solution with a NaCl concentration of 0.6 mol/l, similar to seawater, into a testing chamber, creating a favorable environment for oxidation. The saline solution is applied

to the rail using misting nozzles and a watering programmer. The duration of misting and drying is adjusted according to the desired oxide thickness.

After each oxidation process, the thickness of the oxide layer was measured using a Fischer Deltascope FMP30 probe. This equipment operates on the principle of magnetic induction and is adapted to rough surfaces, with a precision of approximately $\pm 0.2\ \mu m$ for oxide thicknesses of up to $100\ \mu m$.

Figure 6: Appearance of the rail compared to its initial state after a salt spray oxidation protocol.

Figure 6 shows a preliminary oxidation performed on one rail using this system, resulting in severe oxidation, and creating a case with a heavily oxidized zone showcasing an extreme example of an abandoned track. The average oxide thickness, based on more than 30 measurements, is $57\ \mu m$ and a standard deviation of $17\ \mu m$. This oxide thickness exceeds what is typically observed on low-traffic tracks, where oxide thickness varies from 1 to $2\ \mu m$ on the rail tread and 5 to $6\ \mu m$ on the peripheral zone. For the first try, the oxide thickness was intentionally exaggerated since it was difficult to evaluate its influence. Consequently, we aimed at realizing severe rust conditions to ensure deshunting occurrences.

3 Experimental tests: Results and discussion

The tests presented in parts 3.1 to 3.3 were carried out under static conditions (no rolling) and in direct current, using a Keithley 2400 sourcemeter in 4-probe mode to inject current and measure contact resistance.

3.1 Dependence of the resistance on the applied force

This section focuses on the effect of applied force on the contact resistance. In Hertz's theory, the contact resistance as a function of force is predicted to follow a power-law behavior $R_c \sim F^{-\frac{1}{3}}$.

The contact resistance was evaluated with a constant DC current of 0.1 A. The applied load was progressively increased from 30 N to 430 N (maximum force as explained in section 2.2.2), then decreased to 30 N.

Initially the tests were conducted on three zones under normal conditions, in ambient air. In Figure 7, we present the $R_c - F$ characteristics obtained from one of these zones.

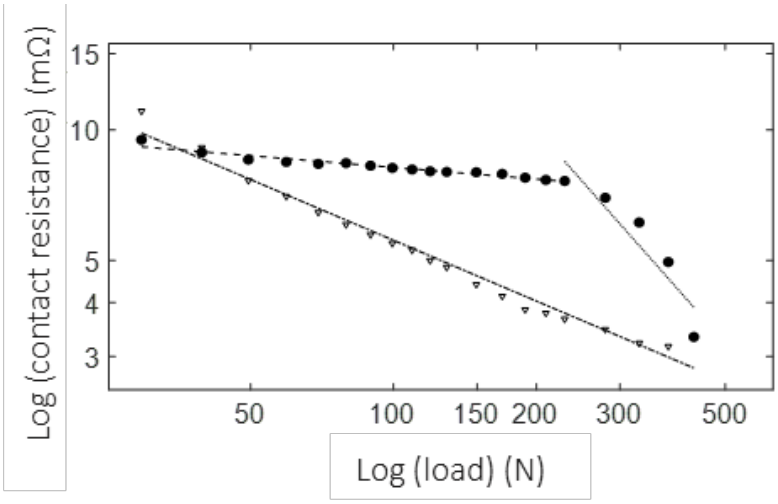

Figure 7: In air - $Log - log\ R_c - F$ characteristics at imposed DC current I=0.1 A when increasing the load (•) from 30 N to 430 N then decreasing it (▽) from 430N to 30N. (- -) shows $F^{-0,09}$ fit of the experimental resistance when increasing force from 30N to 230 N, $(..)$ shows fit $F^{-1.24}$ when increasing force from 230 N to 430 N and $(-.\ )$ shows fit $F^{-0,47}$ when decreasing force from 430 N to 30 N.

These force tests conducted in ambient air reveal unexpected contact resistance behaviours far from those predicted by Hertz. At lower forces (< 230 N), the resistance decreases very slowly, following a power-law $R_c \sim F^{-0.09}$. Beyond 230 N, the resistance exhibits a much more pronounced decrease, following a power-law $R_c \sim F^{-1.24}$ with an exponent greater than one. These observations may reflect the extreme difficulty of obtaining perfectly smooth, clean surfaces on both wheel and rail. Surface roughness, contamination and possible oxidation make it impossible to achieve ideal Hertz's conditions.

3.2 Dependence of the resistance on the applied current

The main objective of this experiment was to explore the impact of the applied current on contact resistance. To this end, contact resistance measurements were carried out on different areas of the rail under static conditions. Increasing and decreasing currents were applied, from 100 mA to 1 A and vice versa, with 100 mA steps every 60 seconds The evolution of the applied current intensity is shown in Figure 8. Contact voltage was measured every second.

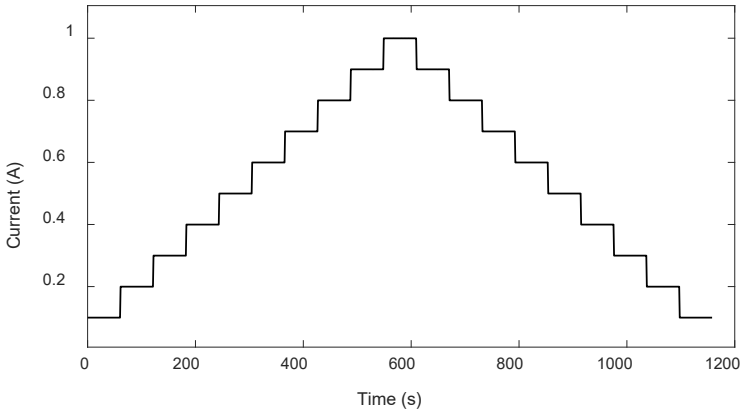

Figure 8: Current I (A) versus time t (s). The current was increased from 0.1 A to 1 A, then decreased from 1 A to 0.1 A by 0.1 A every 60 s.

These tests were conducted on both a clean and an oxidized contact area (oxide thickness=57 μm).

3.2.1. Clean contact: $R_c(I)$

For a clean contact, Figure 9 shows the variation of current and voltage over time. The corresponding *U-I* characteristic is shown in Figure 10. It presents a linear-ohmic and reversible behaviour. In this case, the increasing and decreasing *U-I* characteristics are perfectly superposable on each other. $R_c(I)$ was evaluated at 10 $m\Omega$ which is consistent with a contact on the bare metal.

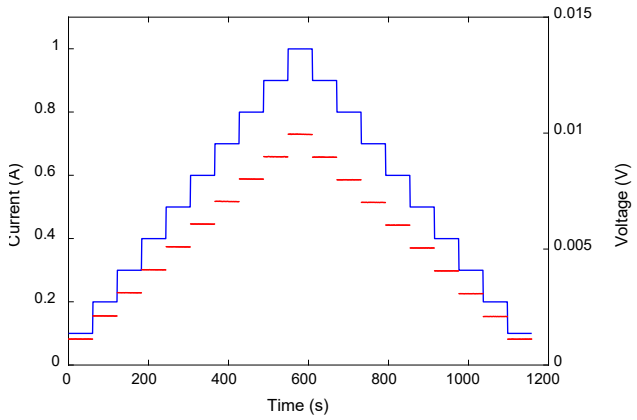

Figure 9: Evolution of the current intensity in the contact (–) and the contact voltage (–) over time for a clean contact between wheel and rail.

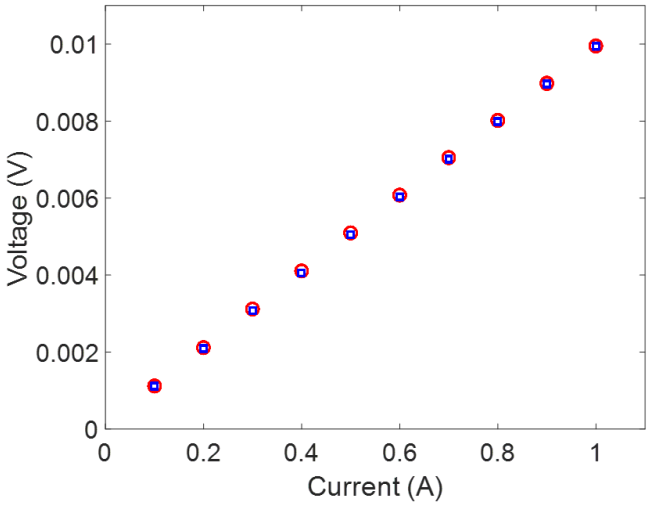

Figure 10: U − I characteristics of a clean contact between wheel and rail when increasing the current I (O) from 0.1 A to 1 A, then decreasing I (□) from 0.1 A to 1 A, for F = 400 N

3.2.2 Oxidized contact: $R_c(I)$

Figure 11 shows the evolution of the current imposed on the contact (similar to the previous case) as a function of time, and the corresponding evolution of the contact voltage in the case of an oxidized surface. Figure 12 and Figure 13 show respectively the evolution of the contact resistance and the *U-I* characteristics during this experiment.

For an oxidized contact, the results reveal a very different behaviour compared to the one observed on the clean contact. Initially, as the current flows, a rapid evolution of the contact occurs, observed as sudden drops in contact resistance with steps of increasing current. This can be observed at the beginning of the curves in Figure 11 and Figure 12: up to 300 seconds and indicates a transition to a less insulating state. This behaviour could be the result of an improved contact due to the flattening of surface asperities under the effect of mechanical stress and the heating generated by the current. As the current continues to increase, the contact resistance gradually stabilizes, indicating a slower evolution of the contact, as shown in Figure 13 after current increase from 0.6 A to 1 A. As the current decreases, $U - I$ characteristics become more linear, and the resistance tends to stabilize at a lower level (approximately 9.8 mΩ) than its previous values. This behaviour is similar to that of a clean contact, as shown Figure 9 and Figure 10, where the voltage is proportional to the current. Overall, the results indicate progressive changes in contact resistance, underlining the influence of current on the electrical properties of an oxidized contact.

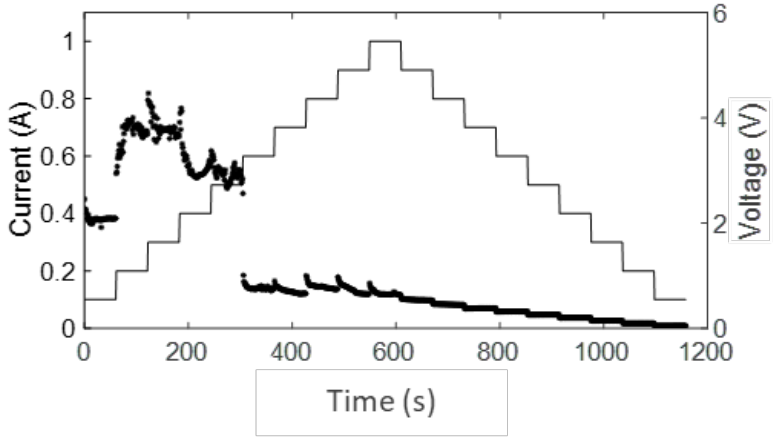

Figure 11: Evolution of the current intensity in the contact (∗ left axis) and the contact voltage (− right axis) over time for an oxidized contact.

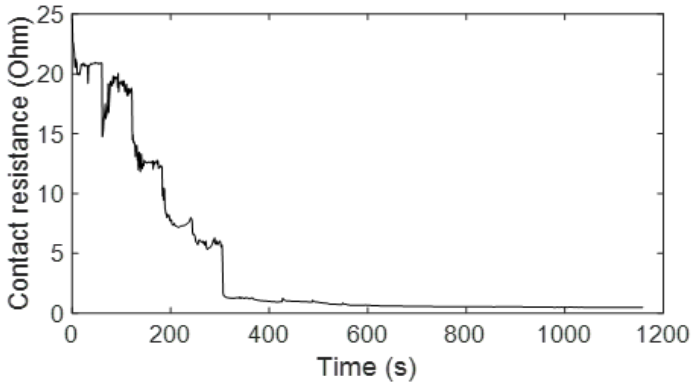

Figure 12: Evolution of the contact resistance over time for an oxidized contact, applying successive steps of increasing and then decreasing current.

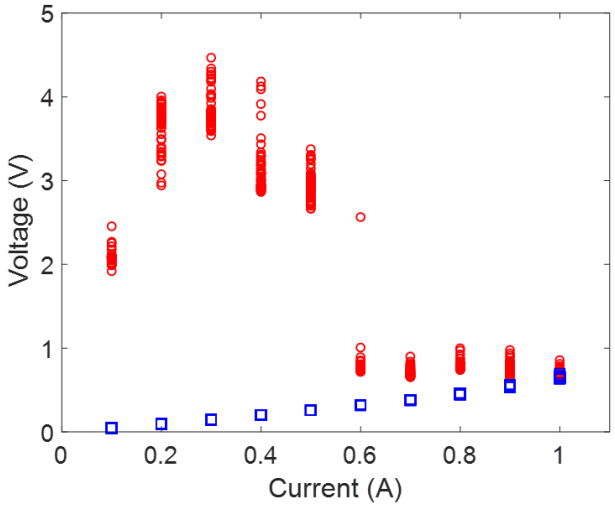

Figure 13*: $U - I$ characteristics of an oxidized contact when increasing the current I (O) from 0.1 A to 1 A, then decreasing I (□) from 0.1 A to 1 A, for F = 400 N.*

4 Conclusion

In this study we designed a scaled-down versatile bench for the study of the wheel-rail electrical contact at a laboratory scale that is able to mimic the wheel rail electrical contact of a train at the laboratory scale. Through a series of preliminary carefully controlled tests, measurements were focused on the influence of contact force, surface roughness, variations in load and oxidation state on the electrical contact. They demonstrated the bench's ability to reproduce phenomena observed on a full scale.

Literature

[1] Wybo J.L, “Track circuit reliability assessment for preventing railway accidents”, Safety Science 1, December 2018. Volume 110, Part B, Pages 268-275

[2] S. Descartes et al., “Presence and role of the third body in a wheel–rail contact”, 2005, Wear, 258, pp. 1081-1090

[3] Suzumura Ja et al. “In situ X-ray analytical study on the alteration process of iron oxide layers at the railhead surface while under railway traffic”. Wear 18 may 2011. Vol. 271, n°1, p. 47 53.

[4] T. Nakahara et al., “Relationship between surface oxide layer and transient traction characteristics for two steel rollers under unlubricated and water lubricated conditions”, 8th International Conference on Contact Mechanics and Wear of Rail/Wheel Systems (CM2009), Firenze, Italia, September 15-18, 2009.

[5] S. Descartes *et al.*, “A new mechanical-electrical approach to the wheel-rail contact”, Wear, vol. 265, pp. 1408-1416, 2008.

[6] M. Fukuda et al., “Study of quantifying and reducing electrical resistance between wheels and rails”, QR of RTRI, vol. 49, n°3, pp. 158-162, 2008.

[7] H. Chollet et al., “Observation of Branly's effect during shunting experiments on scaled wheel-rail contacts”, Proceedings of the 9th International Conference on Contact Mechanics and Wear of Rail/Wheel Systems (CM2012), Chengdu, China, pp. 111-114, 2012.

[8] F. Houzé et al., “Electrical behaviour of the wheel-rail contact”, Proceedings of the 26th Inernational Conference on Electrical Contacts (ICEC-ICREPEC2012), Beijing, China, pp. 67-72, 2012.

[9] Johnson.KL. Contact Mechanics: Cambridge University Press; 1985.

[10] M. Toumi., “Modélisation numérique du contact roue-rail pour l’étude des paramètres influençant les coefficients de Kalker : Application à la dynamique ferroviaire ”, PhD Thesis, Université Paris-Est, 2016.

[11] Timsit R. “Electrical Contact Resistance: Properties of Stationary Interfaces”, IEEE transactions on components and packaging technology, vol. 22, no. 1, March 1999.

[12] Creyssels M. et al., “Experiments and theory of the electrical conductivity of a compressed granular metal”, *AIP Conference Proceedings* 1145, 123–126 ,2009.

[13] Nicodeme C., “ Evaluation de l’adhérence au contact roue-rail par analyse d’images spectrales ”, PhD Thesis, Université Paris sciences et lettres, 2018